Hindawi
Journal of Nanomaterials
Volume 2020, Article ID 9429421, 10 pages
https://doi.org/10.1155/2020/9429421

Research Article

Optimized Loading of TiO_2 Nanoparticles into Electrospun Polyacrylonitrile and Cellulose Acetate Polymer Fibers

Sibongile C. Nkabinde,[1] Makwena J. Moloto,[1] and Kgabo P. Matabola[2]

[1]*Department of Chemistry, Faculty of Applied and Computer Sciences, Vaal University of Technology, Private Bag X021, Vanderbijlpark 1900, South Africa*
[2]*Nanotechnology Innovation Centre, Advanced Materials Division, Mintek, Private Bag X3015, Randburg 2125, South Africa*

Correspondence should be addressed to Makwena J. Moloto; makwenam@vut.ac.za

Received 21 March 2020; Revised 25 May 2020; Accepted 30 May 2020; Published 15 June 2020

Academic Editor: Silvia Licoccia

Polyacrylonitrile (PAN), cellulose acetate (CA), PAN-TiO_2, and CA-TiO_2 nanofibers were prepared using the electrospinning technique under varying the loading of the TiO_2 nanoparticles. The latter TiO_2 nanoparticles were prepared using the sol-gel method by varying the calcination temperatures. The absorption and emission spectra illustrated the formation of TiO_2 nanoparticles with an increase in absorption band edges with smaller particles. The TEM results showed the spherical morphology of the nanoparticles calcined at 500°C with an average diameter of 12.2 ± 3.3 nm. XRD analysis revealed anatase phase as the dominant crystalline phase of the nanoparticles. TiO_2 nanoparticle loadings of 0.2 and 0.4 wt% were incorporated into 16 wt% CA solutions while 1, 2, and 3 wt% of TiO_2 nanoparticles were incorporated into 10 wt% PAN solutions. The SEM results illustrated the lowering in diameter and morphology of the nanofibers upon incorporation of nanoparticles. Their respective average diameters are 220, 338, 181, and 250 nm for PAN, CA, PAN-TiO_2, and CA-TiO_2 polymer fibers, respectively. The morphology of the nanofibers improved while the diameter increased with an increase in polymer concentration. Different loadings of TiO_2 nanoparticles improved the electrospinnability and morphology and further decreased the size of the nanofibers. FTIR spectroscopy signifies the formation of nanocomposites and the presence of TiO_2 nanoparticles which corresponded to the Ti-O stretching and Ti-O-Ti bands on the FTIR spectra.

1. Introduction

With the continuous growth of nanotechnology, nanoscale materials have attracted more attention in the science and research world. Nanomaterials are significant subset materials of nanotechnology with unique and superior properties that differ from materials in a molecular form; these include the physical and chemical properties, also high surface area to volume ratio than their conventional forms [1–3]. Included in the nanoscale materials are the polymer nanofibers, which are defined as fiber materials with a diameter in nanometer to micrometer range [4, 5]. They are favored accounting to their high surface-to-volume ratio, increased mechanical strength, light weight, and controllable pore structures [6]. In the company of different techniques employed to produce fibers, electrospinning is favored because of its ability of fabricating fibers with diameters in micrometer scale and small diameter (nanofibers). Nanofibers produced via electrospinning possess a high surface area to volume ratio and found application in different areas such as bioengineering, nanocatalysis, filtration, and electronics [7, 8].

Electrospinning was first discovered in the early 1930s and has been known since [9]. The process involves the use of electrostatic forces applied on solutions or melts to produce fibers. Electrospinning setup consists of three primary components: a high voltage power supply, a syringe with metallic needle, and a grounded collector [10]. In the usual electrospinning process, a high voltage is applied on the polymer solution, which causes electrostatic charging of the droplet of the polymer [11]. A charged jet of polymer solution is ejected from the tip of the needle when the applied electric

field overcomes the surface tension of the polymer droplets [12]. The interaction between the electric field and the surface tension of the fluid stretches the jet stream, leading to the evaporation of the solvent. This causes the jet stream to be elongated and eventually travels to the grounded collector through spiraling loops forming uniform fibers [5, 13]. The electrospinning process has various parameters that influence the final fiber features [14]. The formation of the electrospun nanofibers is influenced by the process parameters such as tip to collector distance, applied electric field, and the rate at which the solution flows [15, 16]. The morphology and diameter of the electrospun nanofibers depend on the solution parameters such as viscosity, molecular weight, surface tension, and conductivity [17]. Electrospinning is a fast developing technique with many facets ranging from a single-fluid process [18] to other modified coaxial processes [19–21]. Electrospinning provides opportunity to create novel nanomaterials and endow fibers new functional properties.

Research has been conducted on the fabrication of PAN and CA nanofibers using the electrospinning technique and the experimental operational conditions. However, there are a few reports regarding the effect of nanoparticle loading on the morphology and diameter of the fibers. The incorporation of inorganic nanoparticles into polymer nanofibers improves optical, catalytic, electrical, and thermal properties of both the nanofibers and the nanoparticles. These properties of polymer nanofibers depend on the type of incorporated nanoparticles, their size, shape, concentration, and interaction with polymer matrix [8]. Among various nanoparticles, titanium dioxide (TiO_2) has been reported as the most efficient nanomaterial in various areas ranging from wastewater and air treatment to self-cleaning surfaces due to its strong oxidizing power, high photo stability, economical, nontoxicity, and antimicrobial properties, and redox selectivity can be supported on different substrates and its ability to mineralize organic pollutants [22–24]. All these exciting properties of TiO_2 nanoparticles could be introduced into polymers to form nanocomposite materials.

A sol-gel method has been an attractive method for the synthesis of nanoparticles among other methods due to its simplicity, low cost, and the production of desirable structural characteristics of the nanoparticles [19]. Most products obtained via the sol-gel method are amorphous; hence, post-treatment such as the calcination method is preferred to modify the crystal phase, particle size, specific surface area, and morphology of TiO_2 nanoparticles for different applications [25, 26]. South Africa is still one of the countries with abundance of titanium and other minerals. The beneficiation of such mineral is explored by various researchers in many disciplines. Incorporating TiO_2 is just but one of the biological related applications by its incorporation into biocompatible polymer chosen for this study. This study describes the synthesis of TiO_2 nanoparticles using the sol-gel method by varying the calcination temperatures of the nanoparticles with a view to modifying the crystal phase, diameter, and morphological properties of the resultant TiO_2 nanoparticles. The prepared TiO_2 nanoparticles were incorporated into PAN and CA polymers to produce PAN-TiO_2 and CA-TiO_2 polymer nanofibers. Furthermore, the effect of adding different content of TiO_2 nanoparticles on the electrospinnability of PAN and CA was studied.

2. Experimental Section

2.1. Materials. Titanium tetrachloride ($TiCl_4$) (99%), deionized water, NaOH, cellulose acetate (30,000 Mn), PAN ($Mw = 150{,}000\ g \cdot mol^{-1}$), methanol (99% purity), acetone (99% purity), and N,N-dimethylacetamide (DMAc; Assay: 99%). The chemical reagents were supplied by Merck and Sigma-Aldrich, South Africa, and used without further purification or treatment.

2.2. Experimental Procedures

2.2.1. Synthesis of TiO_2 Nanoparticles. The TiO_2 nanoparticles were prepared by slowly adding 6 mL of $TiCl_4$ into 200 mL of distilled water in a 250 mL three-neck round bottomed flask immersed in an ice bath (0°C) and stirred vigorously. The flask was removed from the ice bath and was kept in a magnetic stirrer to make a homogeneous solution for 45 min at 90°C. The solution was cooled and neutralized to a pH of 8.0 using 10 M NaOH to aid the process of gelation then heated again for 30 min while stirring. Centrifugation was used to separate the expected white gel from solution. The precipitate was washed repeatedly with deionized water to remove the chloride ions and methanol to prevent agglomeration between precipitates. After a thorough wash, the precipitate was filtered and allowed to dry at 110°C in an oven overnight. The dried material was crushed into powder using a mortar and pestle and calcined in a programmable furnace at different temperatures of 400, 500, and 600°C for 2 hours.

2.2.2. Preparation of PAN and CA Nanofibers and Their TiO_2 Incorporation. CA was dissolved in a mixture of N,N-dimethylacetamide (DMAc)/acetone (1 : 2 *v*/*v*) to prepare 16 wt% solution for electrospinning. PAN was dissolved in N,N-dimethylacetamide (DMAc) to prepare 10 wt% solution for electrospinning. PAN-TiO_2 nanocomposites were prepared by adding 1, 2, and 3 wt% of TiO_2 nanoparticles. CA-TiO_2 nanocomposites were prepared by adding 0.2 and 0.4 wt% of TiO_2 nanoparticles. Separately, the polymer solutions were delivered through a 20 mL plastic syringe fitted with a stainless steel needle of tip dimensions of 1.20×38 mm at a flow rate of 0.040 mm/min. A high-voltage power supply was used to produce the voltages of 22 kV, and the distance between the nozzle and the collector screen was kept at 15 cm. A stationary metallic roller covered with an aluminum foil was used as a collector for the nanofibers.

2.3. Instrumentation

2.3.1. Optical Characterization. The optical measurements were carried out using a PerkinElmer Lambda 25 UV/VIS spectrophotometer (ELICO-SL-150). The samples were placed in quart cuvettes (1 cm path length) using deionized water as a reference solvent. A PerkinElmer LS 45 Luminescence spectrometer was used to measure the photoluminescence of the particles at the excitation wavelength of

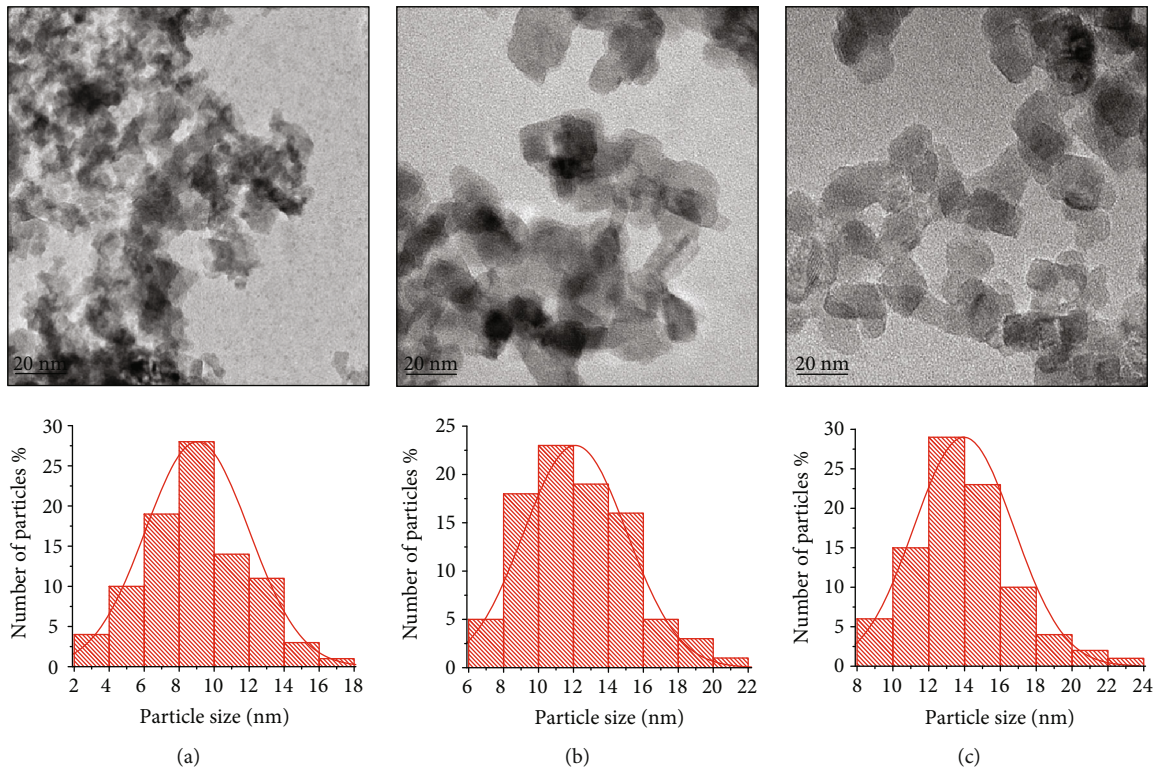

FIGURE 1: TEM images of TiO_2 nanoparticles prepared at different calcination temperatures and the size distribution histogram for samples calcined at (a) 400°C, (b) 500°C, and (c) 600°C, respectively.

320 nm. The samples were placed in glass cuvettes (1 cm path length).

2.3.2. Transmission Electron Microscopy (TEM). TEM images of the synthesized TiO_2 nanoparticles were obtained using a HITACHI JEOL 100S transmission microscope operated at 80 kV. The nanoparticles were diluted in deionized water, and a drop of the solution was placed on a carbon-coated copper grid. The samples were dried at room temperature prior to analysis.

2.3.3. Scanning Electron Microscopy (SEM). The diameter and morphologies of the fibers were studied using the FE-SEM (Leo Zeiss) scanning electron microscopy operated at 1.00 kV electron potential difference. The fibers were carbon-coated before the analysis.

2.3.4. X-Ray Diffraction (XRD). The analysis of the nanomaterials was studied using wide-angle X-ray scattering (WAXS) using a D8-Advance (Bruker miller Co) apparatus. Cukα radiation with a wavelength of $\lambda = 1.54$ Å was used, and measurements were taken at high angle 2θ range of 5-90° with a scan speed of 0.02 q·s^{-1}.

2.3.5. Fourier Transform Infrared (FTIR) Spectroscopy. FTIR spectra of the nanomaterials are obtained from using a Perkin-Elmer spectrum 400 FT-IR spectrometer ranging from 450 to 4000 cm^{-1} with a resolution of 4 cm^{-1}.

2.3.6. Thermal Gravimetric Analysis (TGA). Thermogravimetric analysis of the fibers and the composite fibers was performed using a PerkinElmer STA 6000 simultaneous thermal analyzer under nitrogen with a flow rate of 20°C/min using about 2-4 mg of sample at a temperature range of 30°C to 900°C at a heating rate of 10°C/min.

3. Results and Discussion

3.1. TiO_2 Nanoparticles. TiO_2 nanoparticles were prepared using the sol-gel method as described in the experimental section. The effect of calcination temperature ranging from 400 to 600°C was investigated to check its influence on the formation of the nanoparticles. The sol-gel method increased the possibility of obtaining ultrafine powders which have an extremely large specific surface area. Calcination temperature is one of the major factors influencing the composition, structural, and optical properties of the nanoparticles [25].

3.1.1. Morphological Properties of the Nanoparticles. The TEM images and the size distribution histograms of TiO_2 nanoparticles prepared at different calcination temperatures are shown in Figure 1.

The results showed that the particles are well distributed with less agglomeration, and this is due to the temperature effect. The nanoparticles appear to have spherical shapes with different average particle sizes of 9.1, 12.2, and 14.0 nm at calcination temperatures of 400, 500, and 600°C, respectively. Particle size showed an increase with increasing calcination temperatures, and this could be due to the interaction of many adjoining particles resulting in more spherical large particle sizes by melting their surfaces. Moreover, calcination

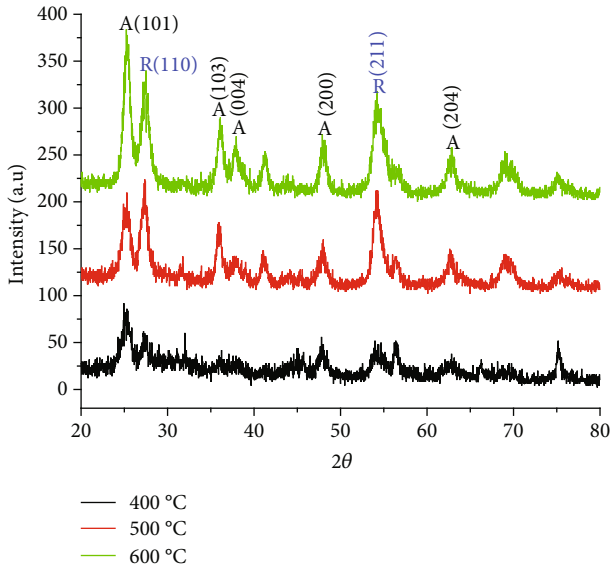

FIGURE 2: XRD patterns of TiO_2 nanoparticles prepared at different calcination temperatures of 400°C, 500°C, and 600°C.

of TiO_2 nanoparticles enhanced the structural and morphological features especially the crystallinity [22].

Figure 2 shows the XRD patterns of TiO_2 nanoparticles calcined at different temperatures of 400, 500, and 600°C. It was observed that, as the calcination temperature increased from 400 to 500°C, the intensity of both anatase and rutile peaks gradually increased and the removal of some small peaks at lower calcination temperature was observed. As the calcination temperature was increased to 600°C, both the anatase and rutile phase became narrower, which indicated the increase of crystallite size, as supported by the TEM images, which is due to the increasing particle size of the TiO_2 nanoparticles. The highest peak at 2θ at 25.5° corresponding to crystal plane (101) of anatase became thinner, and the relative intensity was increased with the increasing calcination temperature.

From the full width at the half maximum of the diffraction pattern, the crystal sizes were calculated by using Scherrer's equation [27]. The crystallite sizes were 8.1, 9.4, and 10.3 nm at calcination temperatures of 400, 500, and 600°C, respectively. The crystallite size increase may be attributed to the increasing calcination temperatures. The narrow sharp peak signifies that the crystalline phase of anatase was formed and an increasing particle size. Strong diffraction peaks representing the anatase phase are observed at 2θ values of 25.5°, 38.2°, 48.1°, and 62.44°, corresponding to the crystal planes of (101), (103), (200), and (105), respectively. Rutile phase was also identified at 2θ values of 27.5°, 41.2°, and 56.5° corresponding to the crystal planes of (110), (200), and (211), respectively.

3.1.2. Optical Properties of the Nanoparticles. Calcination temperature is one of the major factors influencing the structural and optical properties of the TiO_2 nanoparticles. The band gap energy (E_g) of the synthesized TiO_2 nanoparticles was obtained using the following equation:

$$E_g = \frac{1240}{\lambda} \text{eV}, \quad (1)$$

where E_g is the band gap electron volt (eV) and λ is the wavelength of the absorption edges in the spectrum in nanometer (nm) [28].

Figure 3 shows the influence of the calcination temperature on the light absorption characteristics of TiO_2 nanoparticles. The variation of the calcination temperature influences the adsorption edges of the particles.

Figure 3(a) shows an increase in the absorption edges as the calcination temperature was increased from 400, 500, and 600°C with the adsorption edges of 322, 324, and 335 nm, respectively, showing blue shift from the bulk adsorption edge of 388 nm. The synthesized TiO_2 nanomaterials of band gap energy (3.85, 3.83, and 3.70 eV) are larger than the value of 3.2 eV for the bulk TiO_2 nanomaterials. The decrease of the band gap with increasing calcination temperature is due to the increasing nanoparticle size and crystallinity improvement according to the XRD and TEM [28]. The Tauc method was used to calculate the optical band gap of TiO_2 nanoparticles. The Tauc plot gives good approximation of the indirect band gap energy of the nanoparticles. The plot of $(\alpha h\nu)^{1/r}$ against hv reveals a linear region just above the optical absorption edge, where $r = 2$ is used for direct allowed transition, $r = 1/2$ is used for indirect allowed transition, and hv is the photon energy (eV) [25, 29]. Figure 3(b) shows the Tauc plot for band gap calculations. The blue shift in the absorbance spectra of TiO_2 calcined at 400, 500, and 600°C is shown, and absorbance edge corresponds to 344, 342, and 341 nm having band gaps 3.60, 3.62, and 3.64 eV, respectively.

Figure 4 shows the emission peaks of TiO_2 nanoparticles calcined at the above calcination temperatures with an excitation wavelength of 320 nm. Two broad emission peaks appear at 383 nm and 408 nm, which are equivalent to 3.24 eV and 3.04 eV, respectively, showing the red shift from the excitation peak. The difference in the broad PL spectra is due to the various calcination temperatures illustrating the mixed phase structure, surface microstructure, and sizes of the TiO_2 nanoparticles. A significant decrease in the excitonic PL intensity of TiO_2 was observed with increasing calcination temperature due to the increase in particle size and the high crystallinity. The PL spectra also revealed three small peaks at wavelength range from 435 to 538 nm which are attributed to excitonic PL mainly resulting from surface oxygen vacancies of TiO_2 nanoparticles.

3.1.3. FTIR Spectral Analysis of Nanoparticles. Figure 5 shows the FTIR spectra of TiO_2 nanoparticles calcined at different temperatures. The sharp and broad peaks observed in all three spectra at 1690 cm^{-1} and 3400 cm^{-1} correspond to the O-H bending and stretching modes, respectively, indicating adsorbed water molecules in the nanoparticles. The peak at 2954 cm^{-1} corresponds to C-H stretching, which may be

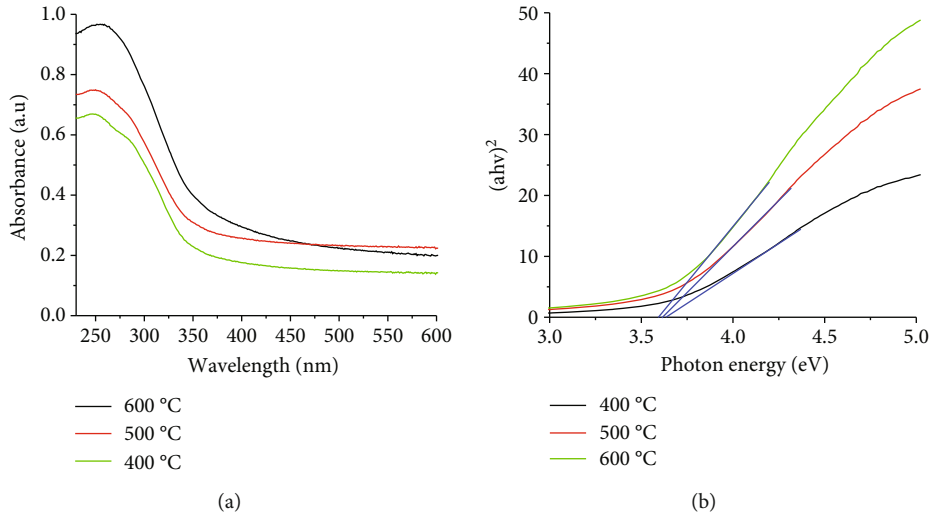

FIGURE 3: (a) Absorption spectra of TiO_2 nanoparticles prepared at different calcination temperatures, 400°C, 500°C, and 600°C. (b) Tauc plot.

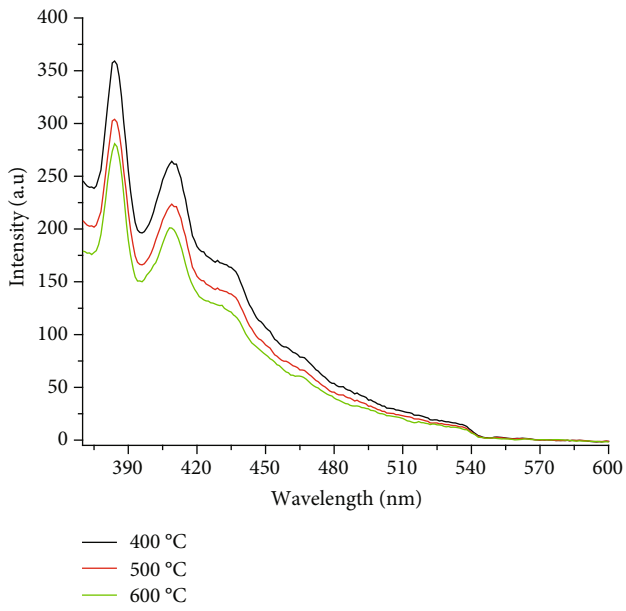

FIGURE 4: PL spectra of TiO_2 nanoparticles prepared at different calcination temperatures of 400°C, 500°C, and 600°C.

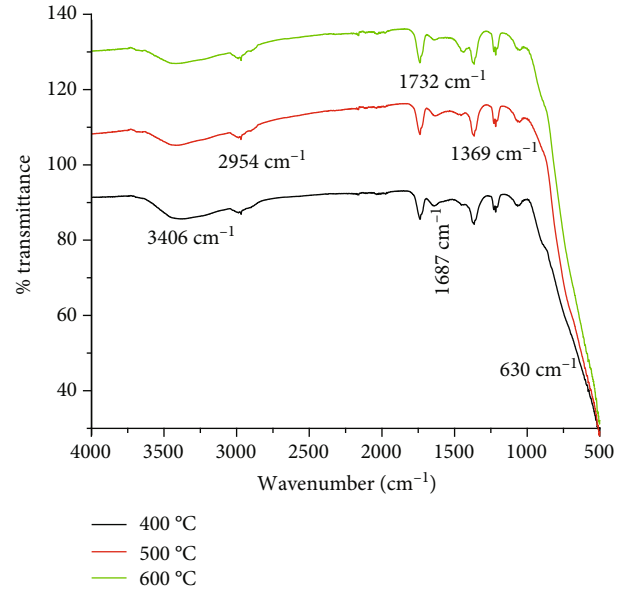

FIGURE 5: FTIR spectra of TiO_2 nanoparticles prepared at different calcination temperatures of 400°C, 500°C, and 600°C.

due to the use of methanol when washing during the preparation of TiO_2 nanoparticles.

The peak in the region from 500 to 900 cm^{-1} is attributed to Ti-O stretching and Ti-O-Ti bridging stretching modes, due to the formation of TiO_2 nanoparticles. The surface absorbance water and hydroxyl group decreased slightly as the calcination temperature increased, and this may be due to the evaporation of a large portion of adsorbed water from TiO_2 and decrease of specific surface area and pore volume.

3.2. Effect of Nanoparticle Loading on the PAN and CA Nanofibers. There are various factors that influence the fabrication of desired fiber morphology and size such as the viscoelasticity of the solution, charge density carried by the jet, and the surface tension of the solution. These factors can be influenced by additives added into the polymer solution. For the incorporation of nanoparticles into polymer fibers, nanoparticles prepared at 500°C calcination temperature were used due to their mixed anatase/rutile phases and spherical shape. Figure 6 shows the effect of TiO_2 nanoparticles loading of 1, 2, and 3 wt % on the morphology and diameter of the electrospun PAN nanofibers. It was observed that the diameter of pure PAN nanofiber (228 nm) was thicker than that of PAN-TiO_2 composite fibers loaded with 1 and 2 wt % TiO_2. The results indicated that the addition of the nanoparticles led to a significant decrease in the fiber diameter.

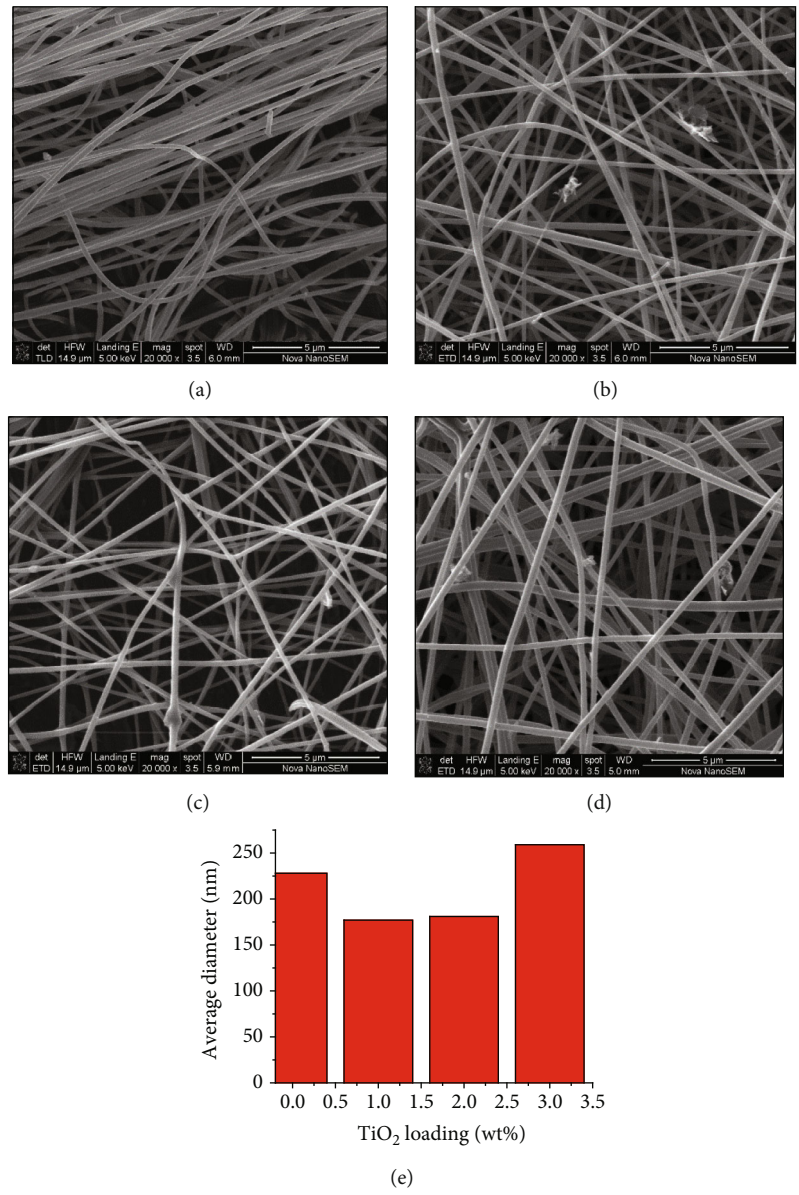

Figure 6: SEM images and average fiber diameter distribution (e) of 10 wt% PAN and different loading of TiO_2 nanoparticles at 10 wt% PAN (a), 1 wt% (b), 2 wt% (c), and 3 wt% (d) electrospun at 15 cm distance and 22 kV voltage.

This could be due to the increased electrical conductivity which led to increased surface charge of the polymer jet, and thus, stronger elongation forces were imposed to the jet, resulting in more uniform fibers with a thinner diameter distribution. Therefore, incorporating TiO_2 nanoparticles into PAN solution enhanced the conductivity of the solution to be electrospun, and as a result of this improved conductivity, the produced fibers became thinner compared with fibers produced from PAN solution. As the concentration of the TiO_2 nanoparticles was further increased to 3 wt%, the fiber morphology improved while the diameter increased to 259 nm which is greater than that of pure PAN. The viscosity of solution is known to influence the reduction process, which is decreased, because a high and optimum concentration of polymer was used in combination with nanoparticle addition. Figure 7 shows the effect of TiO_2 nanoparticle loadings from 0.2 to 0.4 wt% on the morphology and diameter of the electrospun CA nanofibers.

Lower concentration loadings of TiO_2 nanoparticles onto CA were used as compared to the concentration loading of PAN; this is due to the interaction of the nanoparticles with the polymer solution. It was observed that when adding more concentration of TiO_2 nanoparticles onto CA, the solution became more concentrated which hindered the formation of the nanofibers due to the high viscosity, making it difficult to control the flowrate of the polymer solution through the capillary [11, 14]. It is observed that the fiber diameter of pure CA is 338 nm whereas the addition of 0.2 and 0.4 wt % nanoparticles improved fiber morphology with a decreased average diameter of 192 and 250 nm, respectively. This decrease in fiber diameter with the addition of nanoparticles is attributed to the conductivity and charge density increase,

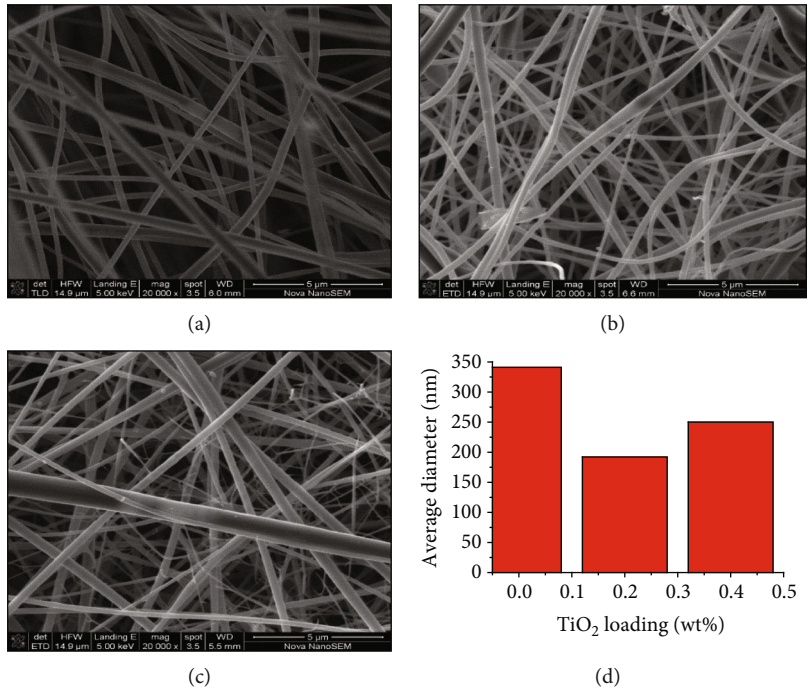

FIGURE 7: SEM images and fiber diameter distribution (d) of 16 wt% CA and different loading of TiO_2 nanoparticles at 16 wt% CA (a), 0.2 wt% (b), and 0.4 wt% (c) electrospun at 15 cm distance and 22 kV voltage.

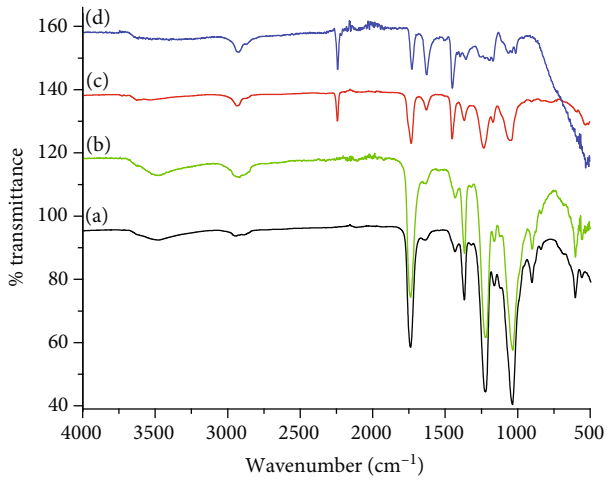

FIGURE 8: FTIR spectra of 16 wt% CA (a), CA-TiO_2 (b), 10 wt% PAN (c), and PAN-TiO_2 (d).

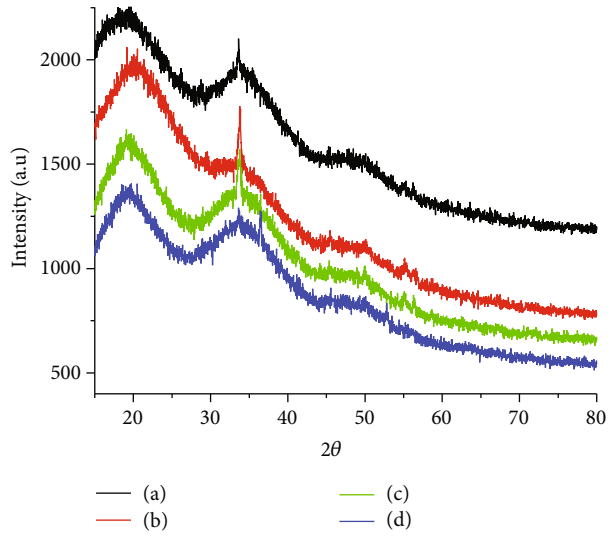

FIGURE 9: XRD patterns of 16 wt% CA (a), CA-TiO_2 (b), PAN-TiO_2 (c), and 10 wt% PAN (d).

resulting in greater stretching and elongation of the jet, thereby causing a reduction in the fiber diameter.

3.2.1. FTIR Spectral Analysis of the Polymer Fibers. Figure 8 shows FTIR spectra of pure CA, pure PAN, CA-TiO_2, and PAN-TiO_2 nanocomposites. The main characteristic bands for CA were assigned as follows: the adsorption peak at 3470 cm^{-1} corresponds to the hydroxyl group, the peak at 2931 cm^{-1} can be attributed to C-H stretching in the CH and CH_2 group, the peak at 1739 cm^{-1} can be attributed to the C=O stretching, 1239 cm^{-1} and 1041 cm^{-1} are due to CH_3, and ether C-O-C functional groups were observed. From the PAN spectra, the peak at 3482 cm^{-1} corresponds to O-H stretching, 2932 cm^{-1} corresponds to C-H stretching in the CH and CH_2 group, 2241 cm^{-1} corresponds to the C≡N stretching, 1750 cm^{-1} is due to C=O stretching, 1453 cm^{-1} is for C-H bending mode, and 1054 cm^{-1} corresponds to C-O stretching mode. Comparing the FTIR spectra of the pure PAN and CA to the CA-TiO_2 and PAN-TiO_2 composites, the characteristic peak of the O-H group was shifted from 3482 cm^{-1} (PAN) and 3470 cm^{-1} (CA) to

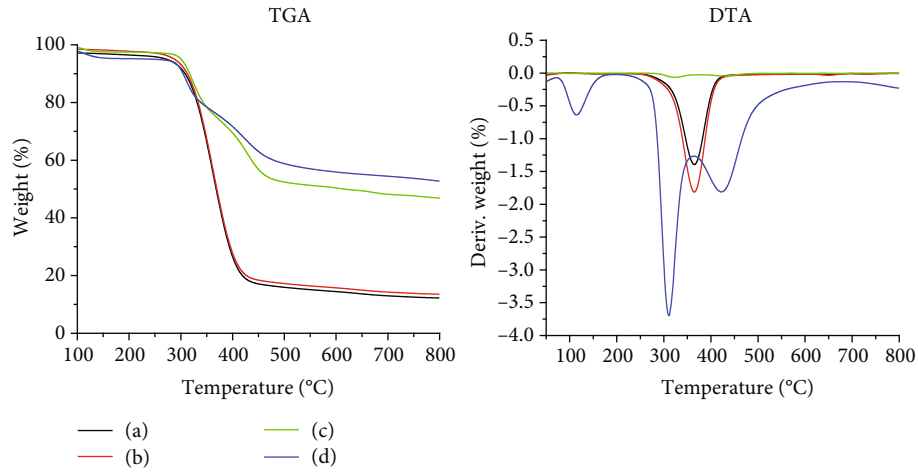

Figure 10: TGA and DTA curves of 16 wt% CA (a), CA-TiO_2 (b), PAN-TiO_2 (c), and 10 wt% PAN (d) polymer fibers.

3531 cm^{-1} (PAN-TiO_2) and 3497 cm^{-1} (CA-TiO_2), respectively. Similar shifts were observed for peaks at 2932 cm^{-1} and 1041 cm^{-1}. The shifts of the peak positions can be attributed to the formation of hydrogen bonding between nanoparticles and matrix. The peak around 500 cm^{-1} corresponds to Ti-O stretching and Ti-O-Ti bands [30, 31].

3.2.2. XRD Analysis of the Polymer Nanofibers. Figure 9 shows the X-ray diffraction patterns of 16 wt% CA, 10 wt% PAN, CA-TiO_2, and PAN-TiO_2. The CA nanofibers reveal two broad amorphous peaks in the range of $2\theta = 15.0$-25.8° and 29.7-40.1° which correspond to its crystalline nature. The XRD patterns of CA nanofibers immobilized with TiO_2 nanoparticles and pure CA nanofibers are similar except the diffraction peak that appears at 33.9° corresponding with (002) plane. The broad peaks centered at $2\theta = 20^\circ$ and 34° observed for PAN and PAN-TiO_2 reveal the amorphous nature of PAN.

PAN-TiO_2 exhibited a diffraction peak of $2\theta = 33.9^\circ$ corresponding with (002) plane. The amount of actual TiO_2 nanoparticles immobilized onto the polymer was most likely too low to be detected using the XRD technique. The PAN-TiO_2 exhibited diffraction peaks around at 28.9°, 31.8°, and 48.0°, corresponding to the (110), (111), and (200) crystal planes of TiO_2, respectively.

3.2.3. TGA Analysis of the Polymer Nanofibers. Figure 10 displays the thermogravimetric analysis of the electrospun composite nanofibers in the temperature range of 30–800°C using 10 mg samples with a heating rate of 10°C/min under a nitrogen purge at a rate of 10 mL/min. The yield residual mass for CA at 800°C was 12.7%, and the initial mass reduction was 3.6% weight loss up to 274°C attributed to the evaporation of water and solvent molecules. The second weight loss was from 274°C to 418°C; it was attributed to cellulose pyrolysis. 17.8% unburned carbonaceous residue was found at 418°C. The TGA curve for CA-TiO_2 has yielded a residual mass of 13.2% at 800°C, and the first mass reduction began at 286°C associated with the evaporation of water. The second degradation occurred from 286°C up to 420°C associated with the main thermal degradation reaction of CA. The TGA curves of CA and CA-TiO_2 were almost the same due to the less amount of TiO_2 nanoparticles incorporated.

The PAN nanofibers' first weight loss was 2.5% from 121°C to 338°C. From 338 to 358°C, the TGA curve showed 21% weight of residue associated with cyclization of nitrile groups in PAN polymer chain [32]. From 358 to 474°C, the TGA curve showed 44% weight loss which might be related to thermal degradation reaction of PAN and the yield residual mass for PAN at 800°C was 52.5%. The PAN-TiO_2 nanofibers' first weight loss was 4.8% from 115 to 144°C. From 144 to 293°C, the weight of PAN was almost unchanged. 19% weight loss up to 352°C was associated with opening of triple bonds. From 352 to 460°C, the TGA curve showed 46% weight of residue associated with decomposition reaction of PAN. The crystallinity of the PAN nanofibers is reduced due to the presence of the nanoparticles. Differential thermal analysis (DTA) provides detailed information on the polymer decomposition temperature.

4. Conclusion

Titanium dioxide nanoparticles were successfully prepared using the sol-gel method under varying calcination temperatures. The successfully synthesized TiO_2 nanoparticles were analyzed using UV-Vis, PL, FTIR spectroscopy, TEM, and XRD. UV-vis spectroscopy confirmed that the TiO_2 nanoparticles formed are nanosized with extended optical band edge. TEM results showed spherical TiO_2 nanoparticles with increased particle size. XRD illustrated the increased crystallite size due to the increase in particle size with increasing calcination temperature. The FTIR spectra confirmed that indeed TiO_2 nanoparticles have been formed as demonstrated by the peak at around 500 cm^{-1} corresponding to Ti-O stretching and Ti-O-Ti bands. The effect of polymer concentration applied voltage and the addition of TiO_2 nanoparticles on the morphology and diameter of the electrospun nanofibers were investigated. SEM images showed the morphology and size of the fabricated polymer nanofibers. Different loadings of TiO_2 nanoparticles improved the

electrospinnability and morphology and decreased the size of the nanofibers. The FTIR spectra confirmed the presence of TiO_2 nanoparticles onto the polymer nanocomposites. This study signified that the addition of TiO_2 nanoparticles into the PAN and CA electrospinning solutions improved the morphology and electrospinnability and further decreased the diameter of the nanocomposite fibers. All the fibers prepared with nanoparticles incorporated in them are air and moisture and thermally stable. Further optimization of the blends as well as the concentration of nanoparticles in those blends will be explored. This will be done in relation to other parameters in electrospinning such as applied voltage and other alternative coaxial processes.

Data Availability

Any additional data to support the findings in their manuscript are available if requested to submit.

Conflicts of Interest

All authors would like to confirm that there are no conflicts of interest with the work and any involvement of other third party except those acknowledged. The article has only been submitted for consideration in this journal and not any other publication.

Acknowledgments

The authors would like to thank Vaal University of Technology and Mintek, for the laboratory space and funding. Great thanks are due to CSIR for their scholarship award to Ms. Sibongile Nkabinde. The authors would like to thank Dr. Pardon Nyamukamba for providing the chemical reagents, polyacrylonitrile and titanium tetrachloride, and Dr. O. Mapazi for providing the reagent, cellulose acetate.

References

[1] P. Sabriye, P. Arzu, and S. Y. Muge, "Antimicrobial activity of synthesised TiO_2 nanoparticles," *International Conference on Emerging Trends in Engineering and Technology*, vol. 7, no. 8, pp. 91–94, 2013.

[2] H. Morteza, H. Mohammad, B. J. Mohammad et al., "Antibacterial effect of TiO_2 nanoparticles on pathogenic strain of E. coli," *International Journal of Advanced Biotechnology and Research*, vol. 3, no. 3, pp. 621–624, 2012.

[3] Y. Yamauchi, T. Nagaura, A. Ishikawa, T. Chikyow, and S. Inoue, "Evolution of standing mesochannels on porous anodic alumina substrates with designed conical holes," *Journal of the American Chemical Society*, vol. 130, no. 31, pp. 10165–10170, 2008.

[4] S. Megelski, J. S. Stephens, D. B. Chase, and J. F. Rabolt, "Micro- and nanostructured surface morphology on electrospun polymer fibers," *Macromolecules*, vol. 35, no. 22, pp. 8456–8466, 2002.

[5] T. Subbiah, G. S. Bhat, R. W. Tock, S. Parameswaran, and S. S. Ramkumar, "Electrospinning of nanofibers," *Journal of Applied Polymer Science*, vol. 96, no. 2, pp. 557–569, 2005.

[6] Z. Tang, C. He, H. Tian et al., "Polymeric nanostructured materials for biomedical applications," *Progress in Polymer Science*, vol. 60, pp. 86–128, 2016.

[7] A. Haider, S. Haider, and I. K. Kang, "A comprehensive review summarizing the effect of electrospinning parameters and potential applications of nanofibers in biomedical and biotechnology," *Arabian Journal of Chemistry*, vol. 11, no. 8, pp. 1165–1188, 2018.

[8] D. S. More, M. J. Moloto, N. Moloto, and K. P. Matabola, "TOPO-capped silver selenide nanoparticles and their incorporation into polymer nanofibers using electrospinning technique," *Materials Research Bulletin*, vol. 65, no. 25, pp. 14–22, 2015.

[9] A. Moheman, M. S. Alam, and A. Mohammad, "Recent trends in electrospinning of polymer nanofibers and their applications in ultra thin layer chromatography," *Advances in Colloid and Interface Science*, vol. 229, pp. 1–24, 2016.

[10] O. S. Yördem, M. Papila, and Y. Z. Menceloğlu, "Effects of electrospinning parameters on polyacrylonitrile nanofiber diameter: an investigation by response surface methodology," *Materials & Design*, vol. 29, no. 1, pp. 34–44, 2008.

[11] P. Nyamukamba, O. Okoh, L. Tichagwa, and C. Greyling, "Preparation of titanium dioxide nanoparticles immobilized on polyacrylonitrile nanofibres for the photodegradation of methyl orange," *International Journal of Photoenergy*, vol. 2016, Article ID 3162976, 9 pages, 2016.

[12] A. Baji, Y. W. Mai, S. C. Wong, M. Abtahi, and P. Chen, "Electrospinning of polymer nanofibers: effects on oriented morphology, structures and tensile properties," *Composites Science and Technology*, vol. 70, no. 5, pp. 703–718, 2010.

[13] X. Shi, W. Zhou, D. Ma et al., "Electrospinning of nanofibers and their applications for energy devices," *Journal of Nanomaterials*, vol. 2015, Article ID 140716, 20 pages, 2015.

[14] K. P. Matabola and R. M. Moutloali, "The influence of electrospinning parameters on the morphology and diameter of poly(vinyledene fluoride) nanofibers- effect of sodium chloride," *Journal of Materials Science*, vol. 48, no. 16, pp. 5475–5482, 2013.

[15] P. Heikkila and A. Harlin, "Parameter study of electrospinning of polyamide-6," *European Polymer Journal*, vol. 44, no. 10, pp. 3067–3079, 2008.

[16] S. Zargham, S. Bazgir, A. Tavakoli, A. S. Rashidi, and R. Damerchely, "The effect of flow rate on morphology and deposition area of electrospun nylon 6 nanofiber," *Journal of Engineered Fibers and Fabrics*, vol. 7, no. 4, 2018.

[17] V. Pillay, C. Dott, Y. E. Choonara et al., "A review of the effect of processing variables on the fabrication of electrospun nanofibers for drug delivery applications," *Journal of Nanomaterials*, vol. 2013, Article ID 789289, 22 pages, 2013.

[18] Y. Yang, T. Zhu, Z. P. Liu, M. Luo, D. G. Yu, and S. W. Annie Bligh, "The key role of straight fluid jet in predicting the drug dissolution from electrospun nanofibers," *International Journal of Pharmaceutics*, vol. 569, pp. 118634–118642, 2019.

[19] H. Zhao, Y. Ma, D. Sun, W. Ma, J. Yao, and M. Zhang, "Preparation and Characterization of Coaxial Electrospinning rhBMP2-Loaded Nanofiber Membranes," *Journal of Nanomaterials*, vol. 2019, Article ID 8106985, 13 pages, 2019.

[20] J. Yang, K. Wang, D.-G. Yu, Y. Yang, S. W. A. Bligh, and G. R. Williams, "Electrospun Janus nanofibers loaded with a drug and inorganic nanoparticles as an effective antibacterial

wound dressing," *Materials Science and Engineering: C*, vol. 111, article 110805, 2020.

[21] K. Zhao, W. Wang, Y. Yang, K. Wang, and D. G. Yu, "From Taylor cone to solid nanofiber in tri-axial electrospinning: size relationships," *Results in Physics*, vol. 15, article 102770, 2019.

[22] S. Singh, H. Mahalingam, and P. K. Singh, "Polymer-supported titanium dioxide photocatalysts for environmental remediation: a review," *Applied Catalysis A: General*, vol. 462-463, pp. 178–195, 2013.

[23] R. S. Devi, D. R. Venckatesh, and D. R. Sivaraj, "Synthesis of titanium dioxide nanoparticles by sol-gel technique," *International Journal of Innovative Research in Science, Engineering and Technology*, vol. 3, no. 8, pp. 15206–15211, 2014.

[24] H. S. Chen, C. Su, J. L. Chen, T. Y. Yang, N. M. Hsu, and W. R. Li, "Preparation and Characterization of Pure Rutile TiO_2 Nanoparticles for Photocatalytic Study and Thin Films for Dye-Sensitized Solar Cells," *Journal of Nanomaterials*, vol. 2011, Article ID 869618, 8 pages, 2011.

[25] N. Wetchakun, B. Incessungvorn, K. Wetchakun, and S. Phanichphant, "Influence of calcination temperature on anatase to rutile phase transformation in TiO_2 nanoparticles synthesized by the modified sol- gel method," *Materials Letters*, vol. 82, pp. 195–198, 2012.

[26] G. Wang, L. Xu, J. Zhang, T. Yin, and H. Han, "Enhanced photocatalytic activity of TiO_2 powders (P 25) via calcination treatment," *International Journal of Photoenergy*, vol. 3, no. 50, 9 pages, 2012.

[27] S. E. Karekar and D. V. Pinjari, "Sonochemical synthesis and characterization of molybdenum sulphide nanoparticles: effect of calcination temperature," *Chemical Engineering and Processing - Process Intensification*, vol. 120, pp. 268–275, 2017.

[28] S. T. Hayle and G. G. Gonfa, "Synthesis and characterization of titanium oxide nanomaterials using sol-gel method," *American Journal of Nanoscience and Nanotechnology*, vol. 2, no. 1, p. 1, 2014.

[29] A. Keiteb, E. Saion, A. Zakaria, N. Soltani, and N. Abdullahi, "A modified thermal treatment method for the up-scalable synthesis of size-controlled nanocrystalline titania," *Applied Sciences*, vol. 6, no. 10, p. 295, 2016.

[30] K. Madhusudan Reddy, S. V. Manorama, and A. Ramachandra Reddy, "Bandgap studies on anatase titanium dioxide nanoparticles," *Materials Chemistry and Physics*, vol. 78, no. 1, pp. 239–245, 2003.

[31] T. Riaz, A. Ahmad, S. Saleemi et al., "Synthesis and characterization of polyurethane-cellulose acetate blend membrane for chromium (VI) removal," *Carbohydrate Polymers*, vol. 153, pp. 582–591, 2016.

[32] H. P. Karki, L. Kafle, D. P. Ojha, J. H. Song, and H. J. Kim, "Cellulose/polyacrylonitrile electrospun composite fiber for effective separation of the surfactant-free oil-in-water mixture under a versatile condition," *Separation and Purification Technology*, vol. 210, pp. 913–919, 2019.